Implicit Multiple-Grid Solution of the Compressible Navier-Stokes Equations Using k-ε Turbulence Closure

G. A. Gerolymos*
LEMFI, Université Pierre et Marie Curie, Paris, France

In the present work, an algorithm for the numerical solution of the two-dimensional mass-weighted, ensemble-averaged, compressible Navier-Stokes equations is presented. Turbulence closure for the Reynolds stresses is obtained using a low-Reynolds-number two-equation k-ε model, which includes near-wall effects. The same algorithm is used for the integration of both the Navier-Stokes and the turbulence-transport equations. The algorithm consists of a basic explicit finite-volume scheme, whose convergence is accelerated using local time-stepping and multiple-grid techniques. Convergence is further enhanced by the use of an implicit-residual-smoothing technique, applied both in the fine and the coarser grids. The application of the numerical scheme to the solution of the k-ε equations is examined in detail. Comparisons of computations with experimental data are presented for three shock-wave/turbulent boundary-layer interaction flows. Algorithm convergence rate and CPU-time requirements are discussed.

Introduction

THE numerical solution of the Navier-Stokes equations for the simulation of turbulent flowfields is a subject of intense research and code development work.[1] Interest is focused both on code applicability to variegated configurations and on computational rapidity. Although direct simulation of turbulent flows[2] or large-eddy numerical simulations using subgrid-turbulence modeling[3,4] have appeared in the literature, current status of algorithm development and computer power indicate that for practical applications the ensemble-averaged Navier-Stokes equations should be used in conjunction with transport equations for turbulence closure.[5-7]

Algebraic or mixing-length models may provide satisfactory results for relatively simple flow geometries[8] but require the determination of the shear-layer thickness and of the distance of each grid point from the solid boundary. Thus, they lack both geometric invariance and locality, which are highly desirable properties, from a computational viewpoint, when addressing complex flowfields with many interacting solid boundaries. Although research on Reynolds-stress-transport closure appears quite promising,[9,10] its extension to three dimensions involves considerable increase of the number of transport equations to be solved. Also, further research concerning wall effects is required, the more so since the use of wall functions is considered inadequate.[11]

On the other hand, the use of two-equation closures, such as k-ε,[12-14] is quite widespread. Notwithstanding the fact that the use of the Boussinesq hypothesis[15] introduces a questionable simplification of the flow physics,[16] the major drawback of the k-ε model is probably the near-wall formulation which fails to reproduce correctly the effects of the solid boundary on turbulence. Several variants of the original Jones-Launder model[12] have been developed in an attempt to improve upon near-wall modeling. Some ten such models have been thoroughly examined in a critical review article by Patel et al.,[17] who concluded that the models of Launder and Sharma,[14] Chien,[18] Lam and Bremhorst,[19] and Wilcox and Rubesin[20] perform better than the others, but need further refinement if they are to be used with confidence to calculate near-wall and low-Reynolds-number flows. The deficiencies of k-ε models, which have been investigated by Bernard[21] and Speziale,[16] may be remedied, however partially, using algebraic Reynolds-stress closures.[22,23] These models perform better than the k-ε, at least in two-dimensional flows,[24] but introduce invariably some ad-hoc asumptions about the flowfield and are not geometrically invariant. In this respect, the proposal to use a nonlinear relationship between the Reynolds-stress tensor and the rate-of-deformation tensor, put forward by Speziale,[16] should be investigated. In the present work, the Lauder-Sharma k-ε model[14] is used. The choice was based, among other reasons, on the fact that its Cartesian-tensor form[23] does not require the knowledge of the grid-point distance from the solid boundaries.

Numerous algorithms for the numerical solution of the compressible Navier-Stokes equations may be found in the literature.[25-30] Most of these algorithms are time marching.[31] For high Reynolds number flows, the convective part of the equations is the most difficult to address. Lomax[32] has discussed a number of ways for accelerating the convergence rate of Navier-Stokes algorithms, such as local time step and multigrid or multiple-grid techniques, which are widely used. The combined use of multigrid and implicit techniques has given quite satisfactory results,[33,34] and is used in this work.

It has often been stated[35,36] that the k-ε equations present serious numerical drawbacks, when coupled with advanced Navier-Stokes algorithms. The purpose of the present work is the development of an efficient compressible Navier-Stokes solver using the Lauder-Sharma[14] k-ε model for turbulence closure. The numerical scheme is based on the explicit Ni's finite-volume scheme followed by the associated multiple-grid scheme.[37,38] An implicit-residual-smoothing technique is used in each grid allowing ($CFL = 3$) local time steps.[39,40] The same numerical scheme is used both for the Navier-Stokes and the k-ε equations.

Flow Model and Turbulence Closure

The flow is modeled by the compressible mass-weighted ensemble-averaged Navier-Stokes equations[41,42]

$$\frac{\partial \boldsymbol{w}}{\partial t} + \frac{\partial \boldsymbol{F}_x}{\partial x} + \frac{\partial \boldsymbol{F}_y}{\partial y} + \boldsymbol{S} = 0 \tag{1a}$$

Received March 27, 1989; revision received Sept. 22, 1989.

*Assistant Professor, Department of Theoretical and Applied Mechanics.

with

$$\boldsymbol{w} = [\rho,\rho u,\rho v,\rho h_t - p]' \tag{1b}$$

$$\boldsymbol{F}_x = [\rho u,\rho uu - \sigma_{xx},\rho vu - \sigma_{yx},\rho h_t u + q_x - u\sigma_{xx} - v\sigma_{yx}]' \tag{1c}$$

$$\boldsymbol{F}_y = [\rho v,\rho uv - \sigma_{xy},\rho vv - \sigma_{yy},\rho h_t v + q_y - u\sigma_{xy} - v\sigma_{yy}]' \tag{1d}$$

$$\boldsymbol{S} = [0,0,0,0]' \tag{1e}$$

where ρ is the density; p the static pressure; u and v the x-wise and y-wise velocity components; h_t the total enthalpy; σ_{xx}, σ_{xy}, σ_{yy}, and σ_{yx} the total stresses; and q_x and q_y the total heat fluxes given by

$$\sigma_{xx} = -p + 2\mu\frac{\partial u}{\partial x} + \lambda\Theta + {}^T\sigma_{xx} \tag{2a}$$

$$\sigma_{xy} = \sigma_{yx} = \mu\left(\frac{\partial u}{\partial y} + \frac{\partial v}{\partial x}\right) + {}^T\sigma_{xy} \tag{2b}$$

$$\sigma_{yy} = -p + 2\mu\frac{\partial v}{\partial y} + \lambda\Theta + {}^T\sigma_{yy} \tag{2c}$$

$$q_x = -\kappa\frac{\partial T}{\partial x} + {}^Tq_x \tag{2d}$$

$$q_y = -\kappa\frac{\partial T}{\partial y} + {}^Tq_y \tag{2e}$$

where Θ is the dilatation $(\partial u/\partial x + \partial v/\partial y)$ and ${}^T(\cdot)$ denotes the turbulent stresses and heat fluxes.

It will be assumed that, in all of the cases which will be examined in the present work, the specific heats c_p and c_v and consequently the isentropic exponent γ may be considered constant with reasonable accuracy, and that the perfect-gas equation of state is applicable

$$p = \rho R_g T \tag{3}$$

where $T = h/c_p$ is the absolute temperature and R_g the gas constant. The dynamic viscosity μ and the heat conductivity κ are assumed to be functions of temperature only,[43] following Sutherland's law[44,45]:

$$\mu = \mu_{273}\left(\frac{T}{273}\right)^{3/2}\frac{273 + S}{T + S} \tag{4a}$$

$$\kappa = \kappa_{273}(1 + AT)\frac{\mu}{\mu_{273}} \tag{4b}$$

The Stokes hypothesis of zero bulk viscosity, $(\lambda = -2\mu/3)$, is adopted.[43,45] For air, using $R_g = 287.04\ \text{m}^2/\text{s}^2/\text{K}$, $\mu_{273} = 17.1\ \mu\text{Pa s}$, $\kappa_{273} = 0.0242\ \text{W/m/K}$, $A = 0.15341 \times 10^{-3}\ \text{K}^{-1}$, $S = 110\ \text{K}$, Eqs. (4) describe quite accurately the evolution of μ and κ from 100–1200 K.[45] Taking into account the evolution of μ and κ is indispensable, since they vary significantly even across transonic boundary layers. The speicfic heats c_p and c_v also vary with temperature, but much less than μ and κ,[45] so that, for transonic boundary layers, their variation may be neglected.

The values of the Reynolds stresses and turbulent heat fluxes, necessary for the closure of Eq. (1), are obtained using the Launder-Sharma[14] k-ε turbulence model

$${}^T\sigma_{xx} = -\frac{2}{3}\rho k + \mu_T\left(2\frac{\partial u}{\partial x} - \frac{2}{3}\Theta\right) \tag{5a}$$

$${}^T\sigma_{xy} = {}^T\sigma_{yx} = \mu_T\left(\frac{\partial u}{\partial y} + \frac{\partial v}{\partial x}\right) \tag{5b}$$

$${}^T\sigma_{yy} = -\frac{2}{3}\rho k + \mu_T\left(2\frac{\partial v}{\partial y} - \frac{2}{3}\Theta\right) \tag{5c}$$

$${}^Tq_x = -\kappa_T\frac{\partial T}{\partial y} \tag{5d}$$

$${}^Tq_y = -\kappa_T\frac{\partial T}{\partial y} \tag{5e}$$

where the values of the eddy viscosity μ_T and the eddy conductivity κ_T are estimated by solving two transport equations for the turbulence kinetic energy k and its dissipation rate ε:

$$\frac{\partial {}^T\boldsymbol{w}}{\partial t} + \frac{\partial {}^T\boldsymbol{F}_x}{\partial x} + \frac{\partial {}^T\boldsymbol{F}_y}{\partial y} + {}^T\boldsymbol{S} = 0 \tag{6a}$$

with

$${}^T\boldsymbol{w} = [\rho k,\rho\varepsilon]' \tag{6b}$$

$${}^T\boldsymbol{F}_x = \left[\rho uk - (\mu + \mu_T/\sigma_k)\frac{\partial k}{\partial x},\rho u\varepsilon - (\mu + \mu_T/\sigma_\varepsilon)\frac{\partial \varepsilon}{\partial x}\right]' \tag{6c}$$

$${}^T\boldsymbol{F}_y = \left[\rho vk - (\mu + \mu_T/\sigma_k)\frac{\partial k}{\partial y},\rho v\varepsilon - (\mu + \mu_T/\sigma_\varepsilon)\frac{\partial \varepsilon}{\partial y}\right]' \tag{6d}$$

$${}^T\boldsymbol{S} = -\left[P_k - \rho\varepsilon + D,C_{\varepsilon_1}P_k\frac{\varepsilon^2}{k} - C_{\varepsilon_2}f_{\varepsilon_2}(Re_T)\frac{\varepsilon^2}{k} + E\right]' \tag{6e}$$

with

$$P_k = {}^T\sigma_{xx}\frac{\partial u}{\partial x} + {}^T\sigma_{xy}\left[\frac{\partial u}{\partial y} + \frac{\partial v}{\partial x}\right] + {}^T\sigma_{yy}\frac{\partial v}{\partial y} \tag{6f}$$

$$Re_T = \frac{\rho k^2}{\mu\varepsilon}, \qquad f_\mu = \exp\left[\frac{-3.4}{(1 + Re_T/50)^2}\right] \tag{6g}$$

$$\mu_T = \{C_\mu f_\mu(Re_T)Re_T\}\mu, \qquad \kappa_T = \frac{c_p\mu_T}{Pr_T} \tag{6h}$$

$$D = -2\mu[\nabla(\sqrt{k})]^2, \qquad E = 2\frac{\mu\mu_T}{\rho}[\nabla^2(V)]^2 \tag{6i}$$

$$f_{\varepsilon_2}(Re_T) = 1 - 0.3e^{-Re_T^2}, \qquad C_\mu = 0.09,$$
$$C_{\varepsilon_1} = 1.44, \qquad C_{\varepsilon_2} = 1.92 \tag{6j}$$

$$\sigma_k = 1, \qquad \sigma_\varepsilon = 1.3, \qquad Pr_T = 0.9 \tag{6k}$$

where Re_T is the turbulence Reynolds number; P_k the turbulence kinetic energy production; C_μ, C_{ε_1}, C_{ε_2}, σ_k, σ_ε, and Pr_T are model constants; and f_μ and f_{ε_2} are functions of the turbulence Reynolds number modeling, the low Reynolds-number effects. The terms D and E model the near-wall effects. The details concerning the preceding turbulence closure may be found in the original references[12–14] and in various review articles.[10,17] It should be noted that the Cartesian tensor form E given by Laksminararayana[23] is slightly different than the one used in this work, but gives practically identical results.

A note on the range of applicability of the flow model used in the present work is of order here. There is no substantial Reynolds-number restriction since the turbulence closure used is well-adapted to transitional flows, as well as fully turbulent ones. However the applicability of the turbulence closure used is restricted in the Mach-number range in which the Morkovin hypothesis[46] is valid, namely from $(M \to 0)$ to $(M \cong 5)$.[47] For higher Mach-number values, that is, in the hypersonic flow regime, the effects of compressibility on turbulence become dependent upon the density fluctuations, which should therefore be taken into account in the modeling.[48]

Numerics

Method Organization

The numerical algorithm solves the Navier-Stokes equations [Eqs. (1)] and the k-ε turbulence transport equations [Eq. (6)]. These two sets of equations are solved simultaneously but separately so as to allow for code modularity with respect to turbulence modeling. At every iteration cycle, the Navier-Stokes solution is advanced in time using the previous iteration k-ε values for the determineation of the Reynolds stresses. Then, after the application of boundary conditions for the mean-flow quantities, the k-ε field is advanced in time using the new flowfield values. The subsequent application of the k-ε boundary conditions marks the end of the iteration cycle, which is then repeated, until convergence is reached. A similar procedure was used by Sahu and Danberg.[49] The iteration cycle of the numerical scheme is described in the following for the Navier-Stokes equations with a fictitious source term [Eqs. (1)], their structure being identical to the k-ε equations [Eqs. (6)]. Since only steady-state flows are considered in the present work, time consistency of the numerical scheme may be relaxed for the purpose of accelerating convergence. Thus, local-time-step and non-time-consistent multiple grid techniques are used.

Numerical Scheme

The mathematical formulation of the numerical scheme and the associated grid features and nomenclature are presented in Fig. 1 and Table 1. The scheme consists mainly of two consecutive sections. The first one is a driver explicit scheme with implicit residual smoothing so as to allow the use of ($CFL = 3$) local time steps. The second section is a multiple-grid algorithm driven by the residuals of the basic scheme. The multiple-grid algorithm uses implicit residual smoothing so as to allow ($CFL = 3$) local time steps on each coarser grid.

The explicit scheme in Table 1 (step 1.1) is the finite-volume scheme developed by Ni.[37,38] The scheme would be second-order accurate both in time and space, if the flux gradient $\partial \boldsymbol{F}/\partial \boldsymbol{w}$ were evaluated including the viscous terms. Nevertheless, this would lead to quite complicated expressions, including interactive feedback with the turbulence model, so that it is usual practice to compute only the advective part of the flux gradient.[38,50] The expression of $\partial \boldsymbol{F}/\partial \boldsymbol{w}$ may be found in the literature.[37,38,50] This practice, which does not affect significantly the steady-state result, was adopted in the present work. The scheme computes approximations to the first and second time derivatives of the unknowns and estimates the new values of the unknowns using second-order Taylor expansions in time. Then, a fourth-order smoothing (step 1.2.1) and a second-order nonlinear shock-capturing dissipation (step 1.2.2) are applied. These artificial dissipation terms (damping terms) stabilize the numerical scheme by modifying its truncation error.[51] This explicit scheme is stable under the restriction of ($CFL \leq 1$) local time steps. In order to use larger time steps so as to accelerate convergence, implicit schemes must be used.[25, 29,30] However, the implicit residual-smoothing finite-volume technique developed by Lerat[39] and Sides[40] is an interesting alternative due to its simplicity and small computing-time requirements. It modifies, via an implicit procedure, the truncation error of the scheme in order to insure stability for ($CFL > 1$) local time steps. The implicit residual-smoothing technique is used in the present work (step 1.3) and has made possible the use of ($CFL = 3$) local time steps. Since the implicit residual smoothing modifies only the truncation error of the scheme, the viscous terms may be neglected in this step, without substantial modification of the converged solution. Note that $\boldsymbol{V}$ is the velocity vector and a is the velocity of sound (Table 1).

The residuals computed by the driver scheme are propagated in the flowfield using the multiple-grid finite-volume technique developed by Ni.[37] In this technique, a number of coarser grids, obtained from the basic grid by omission of every second point in each direction, are used. The finer-grid residuals are transferred to the immediately coarser grid (step 2.1.1), where second time derivatives are computed to evaluate new residuals (step 2.1.2). Following Johnson,[52] the time changes of the viscous terms are neglected in the multiple-grid section. This renders the multiple-grid algorithm nonconsistent with the equations, but has no effect on the converged solution, since the multiple-grid step is driven by the fine-grid scheme residuals.[37,50,52] The multiple-grid scheme (step 2.1.2) is explicit, hence subject to the ($CFL \leq 1$) stability condition. In the present work, the implicit residual-smoothing technique (step 2.1.3) is applied on the residuals of each coarser grid, making possible the use of ($CFL = 3$) local time steps on each grid. This procedure (step 2.1) is repeated until the coarsest grid is reached. Then the computed coarse-grid time changes are cumulatively interpolated into the fine grid (step 2.2).

The procedure just described constitutes one iteration cycle. An assessment of the relative merits of each technique and the associated convergence enhancement is presented in the section on "Convergence and Computing-Time Requirements."

Note on the k-ε Equations

The turbulence transport equations [Eqs. (6)] are integrated in exactly the same way as the Navier-Stokes equations [Eqs. (1)]. Identical time steps are used for both sets of equations, based on a ($CFL = 3$) criterion for the Navier-Stokes equations. It should be noted, both for the driver scheme and the multiple-grid procedure, that taking into account the second-order changes of the source terms is essential for the stability of the method. The derivatives $\partial^T \boldsymbol{S}/\partial^T \boldsymbol{w}$ are computed using the following equations:

$$\frac{\partial S_k}{\partial \rho k} = -\frac{2P_k}{\rho k} \tag{7a}$$

$$\frac{\partial S_k}{\partial \rho \varepsilon} = 1 + \frac{P_k}{\rho \varepsilon} \tag{7b}$$

$$\frac{\partial S_\varepsilon}{\partial \rho k} = -[C_{\varepsilon_1} P_k + C_{\varepsilon_2} f_{\varepsilon_2}(Re_T)\rho\varepsilon]\frac{\rho\varepsilon}{(\rho k)^2} \tag{7c}$$

$$\frac{\partial S_\varepsilon}{\partial \rho \varepsilon} = 2C_{\varepsilon_2} f_{\varepsilon_2}(Re_T)\frac{\varepsilon}{k} \tag{7d}$$

The source terms are neglected in the implicit step. Also, the spectral radius of the implicit residual-smoothing step (Table 1) is $|{}^n\boldsymbol{V}^{11}\boldsymbol{s}_i|$ and not $(|{}^n\boldsymbol{V}^{11}\boldsymbol{s}_i| + {}^n a)$, when considering the k-ε equations.

It is known[53] that the k-ε equations are instability prone during the transitory phase of the computations, when the leading part of the error surges out of the computational domain, generating large residuals. This is why, often,[54,55] the k-ε computations are started from a previously computed, using algebraic-turbulence modeling, initial flowfield. Nevertheless, such a technique is not practicable for complex configurations. In the present study, the voluntarily uncoupled way in which the mean flow and the turbulence transport equations are solved does not ameliorate the situation, nor does neglecting the source terms in the implicit step (Table 1). In order to stabilize the computations k and ε were bounded by the following limiters:

$$k \geq k_{\min} > 0 \tag{8a}$$

$$\varepsilon \geq \varepsilon_{\min} > 0 \tag{8b}$$

$$0.1P_k \leq \rho\varepsilon \leq 10P_k \tag{8c}$$

where $k_{\min}$ and $\varepsilon_{\min}$ are very small positive values intended to prevent k and ε from becoming negative near the wall during the transitory phase of the iterations, and Eq. (8c) imposes $\rho\varepsilon$ to be of the same order of magnitude as P_k so as to avoid instabilities near the boundary-layer edge. These limiting pro-

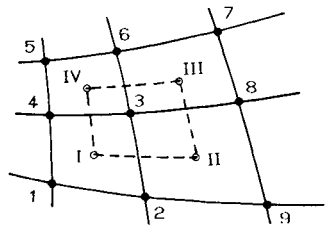

a)

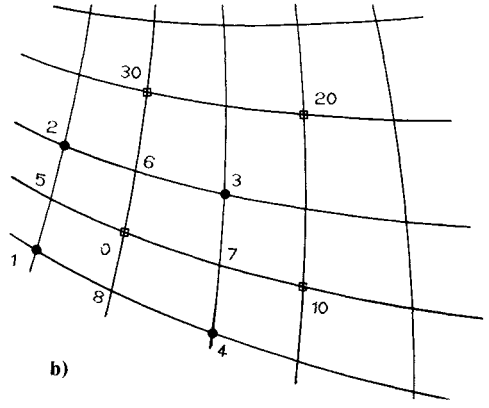

b)

Fig. 1 a) Driver scheme (● grid-point, ○ volume centers, —— grid-lines, - - - translated volume for second-order time changes); and b) multiple-grid technique (—— h-grid, ● 2h-grid-points, □ volume-centers for 2h-grid).

Table 1 Numerical scheme

0. Numerical operators

0.1 Difference operators

$$\Delta(\cdot) = {}^{n+1}(\cdot) - {}^{n}(\cdot) \qquad {}^{ab}\delta_i = (\cdot)_{i+a} - (\cdot)_{i-b}$$

0.2 Metrics

$${}^{ab}l_i = ({}^{ab}\delta_i x)^2 + ({}^{ab}\delta_i y)^2 \qquad {}^{ab}\text{vol} = \tfrac{1}{2}[(x,y)_{i+a,j+a} - (x,y)_{i-b,j-b}] \times [(x,y)_{i-b,j+a} - (x,y)_{i+a,j-b}]$$

$${}^{ab}s_{i_x} = {}^{ab}\delta_j y / {}^{ab}l_j \qquad (\cdot)_i = (\cdot)_x\, {}^{10}s_{i_x} + (\cdot)_y\, {}^{10}s_{i_y}$$

$${}^{ab}s_{i_y} = -{}^{ab}\delta_j x / {}^{ab}l_j \qquad (\cdot)_j = (\cdot)_x\, {}^{10}s_{j_x} + (\cdot)_y\, {}^{10}s_{j_y}$$

$${}^{ab}s_{j_x} = -{}^{ab}\delta_i y / {}^{ab}l_i$$

$${}^{ab}s_{j_y} = {}^{ab}\delta_i x / {}^{ab}l_i$$

0.3 Scheme operators

$$\frac{\text{D}|\text{C}}{\text{A}|\text{B}} \quad \text{MEAN}(\cdot) = \tfrac{1}{4}[(\cdot)|_{\text{A}} + (\cdot)|_{\text{B}} + (\cdot)|_{\text{C}} + (\cdot)|_{\text{D}}]$$

$$\frac{\text{D}|\text{C}}{\text{A}|\text{B}} \quad \text{DIV}(\boldsymbol{F}) = \tfrac{1}{2}[-(\boldsymbol{F}_i|_{\text{A}} + \boldsymbol{F}_i|_{\text{D}})\,{}^{10}l_j|_{\text{A}} + (\boldsymbol{F}_i|_{\text{B}} + \boldsymbol{F}_i|_{\text{C}})\,{}^{10}l_j|_{\text{B}} - (\boldsymbol{F}_j|_{\text{A}} + \boldsymbol{F}_j|_{\text{B}})\,{}^{10}l_i|_{\text{A}} + (\boldsymbol{F}_j|_{\text{D}} + \boldsymbol{F}_j|_{\text{C}})\,{}^{10}l_i|_{\text{D}}]$$

$$\text{DSM}(\cdot) = (\cdot)_{i+2} - 4(\cdot)_{i+1} + 6(\cdot)_i - 4(\cdot)_{i-1} + (\cdot)_{i-2}$$

$$\text{DNL}(\cdot) = (\rho_{i+1} + \rho_i)\,{}^{10}\delta_i(\cdot)|\,{}^{10}\delta_i(\cdot)| + (\rho_{i-1} + \rho_i)\,{}^{01}\delta_i(\cdot)|\,{}^{01}\delta_i(\cdot)|$$

1. Driver scheme (Fig. 1a)

1.1 Ni explicit finite-volume scheme

$$\Delta t|_{\text{I}} = \frac{4|3}{1|2}\ \text{MEAN}(\Delta t) \qquad {}^{10}l_i|_{\text{I}} = \frac{2|3}{2|3}\ \text{MEAN}({}^{11}l_i)$$

$$\boldsymbol{S}|_{\text{I}} = \frac{4|3}{1|2}\ \text{MEAN}(\boldsymbol{S}) \qquad \left.\frac{\partial \boldsymbol{F}}{\partial \boldsymbol{w}}\right|_{\text{I}} = \frac{4|3}{1|2}\ \text{MEAN}\left(\frac{\partial \boldsymbol{F}}{\partial \boldsymbol{w}}\right)$$

$$\left.\frac{\partial \boldsymbol{w}}{\partial t}\right|_{\text{I}} = -\frac{\Delta t|_{\text{I}}}{{}^{10}\text{vol}|_{\text{I}}}\ \frac{4|3}{1|2}\ \text{DIV}(\boldsymbol{F}) - (\Delta t \boldsymbol{S}|_{\text{I}})$$

$$\left.\frac{\partial \boldsymbol{w}}{\partial t}\right|_3 = \frac{\text{IV}|\text{III}}{\text{I}|\text{II}}\ \text{MEAN}\left(\frac{\partial \boldsymbol{w}}{\partial t}\right) \qquad \left[\frac{\partial \boldsymbol{S}}{\partial \boldsymbol{w}}\frac{\partial \boldsymbol{w}}{\partial t}\right]_3 = \frac{\text{IV}|\text{III}}{\text{I}|\text{II}}\ \text{MEAN}\left[\frac{\partial \boldsymbol{S}}{\partial \boldsymbol{w}}\frac{\partial \boldsymbol{w}}{\partial t}\right]$$

$$\left.\frac{\partial^2 \boldsymbol{w}}{\partial t^2}\right|_3 = -\frac{2\,\Delta t|_3}{{}^{11}\text{vol}|_3}\ \frac{\text{IV}|\text{III}}{\text{I}|\text{II}}\ \text{DIV}\left[\frac{\partial \boldsymbol{F}}{\partial \boldsymbol{w}}\frac{\partial \boldsymbol{w}}{\partial t}\right] - \Delta t|_3\left[\frac{\partial \boldsymbol{S}}{\partial \boldsymbol{w}}\frac{\partial \boldsymbol{w}}{\partial t}\right]_3$$

$${}^{\text{NI}}\boldsymbol{w} = {}^{n}\boldsymbol{w} + \Delta t\frac{\partial \boldsymbol{w}}{\partial t} + \frac{\Delta t^2}{2}\frac{\partial^2 \boldsymbol{w}}{\partial t^2}$$

1.2 Smoothing and artificial dissipation

1.2.1 Fourth-order smoothing

$$^{SM}w = {}^{NI}w - q_{SM}[DSM_i({}^{n}w) + DSM_j({}^{n}w)]$$

1.2.2 Nonlinear shock-capturing dissipation

$$^{exp}(\rho V) = {}^{SM}(\rho V) + q_{NL}[DNL_i({}^{n}V) + DNL_j({}^{n}V)]$$

1.3 Implicit residual smoothing

$$a_{-1}\,{}^{*}\Delta w_{i-1,j} + a_0\,{}^{*}\Delta w_{i,j} + a_{+1}\,{}^{*}\Delta w_{i+1,j} = {}^{exp}\Delta w_{i,j}$$

$$b_{-1}\,{}^{dr}\Delta w_{i,j-1} + b_0\,{}^{dr}\Delta w_{i,j} + b_{+1}\,{}^{dr}\Delta w_{i,j+1} = {}^{*}\Delta w_{i,j}$$

$$a_{\pm 1} = \frac{\beta}{{}^{11}\mathrm{vol}}\left\{\left[\frac{\Delta t^2}{{}^{11}\mathrm{vol}}[(|{}^{n}V^{11}s_i| + {}^{n}a)l_j]^2\right]_i + \left[\frac{\Delta t^2}{{}^{11}\mathrm{vol}}[(|{}^{n}V^{11}s_i| + {}^{n}a)l_j]^2\right]_{i\pm 1}\right\}$$

$$a_0 = 1 - a_{-1} - a_{+1}, \qquad \beta = -1$$

2. Multiple-grid scheme (Fig. 1b)

2.1 Coarse grid propagation

2.1.1 Transfer of residuals from h-grid to 2h-grid

$$({}^{2h}_{h}T\,{}^{h}\Delta w)|_0 = \frac{1}{4}\,{}^{h}\Delta w|_0 + \frac{1}{4}\,\begin{matrix}4\\1\end{matrix}\,\Big|\,\begin{matrix}3\\2\end{matrix}\ \mathrm{MEAN}({}^{h}\Delta w) + \frac{1}{2}\,\begin{matrix}8\\5\end{matrix}\,\Big|\,\begin{matrix}7\\6\end{matrix}\ \mathrm{MEAN}({}^{h}\Delta w)$$

2.1.2 Coarse grid changes

$$\frac{\partial F}{\partial w}\bigg|_0 = \begin{matrix}4\\1\end{matrix}\,\Big|\,\begin{matrix}3\\2\end{matrix}\ \mathrm{MEAN}\left(\frac{\partial F}{\partial w}\right), \qquad {}^{2h}\Delta t = 2^{h}\Delta t$$

$$\left[\frac{\partial S}{\partial w}({}^{2h}_{h}T\,{}^{h}\Delta w)\right]_3 = \begin{matrix}30\\0\end{matrix}\,\Big|\,\begin{matrix}20\\10\end{matrix}\ \mathrm{MEAN}\left[\frac{\partial S}{\partial w}({}^{2h}_{h}T\,{}^{h}\Delta w)\right]$$

$${}^{2h}\Delta w|_3 = -\frac{{}^{2h}\Delta t|_3}{\begin{matrix}10\\2h\end{matrix}\ \mathrm{vol}|_1}\ \begin{matrix}30\\0\end{matrix}\,\Big|\,\begin{matrix}20\\10\end{matrix}\ \mathrm{DIV}\left[\frac{\partial F}{\partial w}({}^{2h}_{h}T\,{}^{h}\Delta w)\right] - {}^{2h}\Delta t|_3\left[\frac{\partial S}{\partial w}({}^{2h}_{h}T\,{}^{h}\Delta w)\right]_3$$

2.1.3 Coarse grid implicit residual smoothing

Step 1.3 on ${}^{2h}\Delta w$ on 2h-grid

2.1.4 Transfer to coarser grid

Repeat steps 2.1.1, 2.1.2, 2.1.3 until the coarsest grid is reached

2.2 Residual interpolation to fine grid

2.2.1 Interpolation of residuals from 2h-grid to h-grid

$${}^{h}\Delta w|_0 = {}^{h}\Delta w|_0 + \begin{matrix}4\\1\end{matrix}\,\Big|\,\begin{matrix}3\\2\end{matrix}\ \mathrm{MEAN}({}^{2h}\Delta w)$$

$${}^{h}\Delta w|_5 = {}^{h}\Delta w|_5 + \begin{matrix}1\\1\end{matrix}\,\Big|\,\begin{matrix}2\\2\end{matrix}\ \mathrm{MEAN}({}^{2h}\Delta w)$$

$${}^{h}\Delta w|_8 = {}^{h}\Delta w|_8 + \begin{matrix}1\\1\end{matrix}\,\Big|\,\begin{matrix}4\\4\end{matrix}\ \mathrm{MEAN}({}^{2h}\Delta w)$$

2.2.2 Interpolation of residuals to finer grid

Repeat step 2.2.1 until the finest grid is reached

cedures fully stabilized the computations and made possible the use of a simple initialization of the flowfield.

Grid Generation

Although the finite-volume method may be extended to nonstructured grids,[56] in the present work only fully structured grids were considered, that is grids where the number of points I-wise is the same at every J-station, and vice versa. These grids are simpler to code and present advantages in vectorization for supercomputers. The numerical grid is generated automatically by solving elliptic partial differential equations[57,58]:

$$(x_\eta^2 + y_\eta^2)x_{\xi\xi} - 2(x_\xi x_\eta + y_\eta y_\xi)x_{\xi\eta} + (x_\xi^2 + y_\xi^2)x_{\eta\eta} = 0 \quad (9a)$$

$$(x_\eta^2 + y_\eta^2)y_{\xi\xi} - 2(x_\xi x_\eta + y_\eta y_\xi)y_{\xi\eta} + (x_\xi^2 + y_\xi^2)y_{\eta\eta} = 0 \quad (9b)$$

where x,y are the Cartesian coordinates, and ξ,η the I-wise and J-wise curvilinear coordinates, respectively. This nonlinear elliptic partial differential equation [Eqs. (9)] is solved by iterative underrelaxation,[59] using the finite-volume technique. Grid clustering was simply obtained by interpolation in a uniform initial grid.[60]

Such structured grids are often inadequate for complex geometric configurations. In order to overcome this difficulty, the subdomain approach[61] may be used. In this approach, the flow domain is partitioned to a number of subdomains and structured grids are generated in each subdomain. Information is exchanged between adjacent subdomains at every iteration of the solution procedure, as part of the boundary conditions applied on each subdomain.

Initialization

An initial flowfield is required to start up the time-marching computation.[31] In the present work, the flowfield is initialized by an approximate inviscid flow which conforms with the boundary conditions on the contour of the computational domain and is estimated in the interior by bilinear interpolation of the contour values.

At the proximity of solid boundaries, adiabatic flat-plate zero pressure-gradient velocity and temperature profiles are fitted using semiempirical laws. These are based on an equivalent incompressible velocity profile, following the law developped by Kuhn and Nielsen[62]:

$$u^* = u_\tau[2.5\,\ell n(1 + y^+) + 5.1 - (3.39y^+ - 5.1)e^{-0.37y^+}] \quad (10)$$

where u_τ is the friction velocity $[\mathrm{sign}(\tau_w)\sqrt{(|\tau_w|/\rho)}]$, and y^+ is the wall-distance parameter ($y^+ = yu_\tau/\nu_w$). The equivalent incompressible velocity is related to the actual one through the van Driest transformation[63,64]:

$$u^* = u_e\alpha^{-1}\arcsin(\alpha u/u_e) \quad (11a)$$

with

$$\alpha^2 = r\frac{\gamma - 1}{2}M_e^2\Big/\left(1 + r\frac{\gamma - 1}{2}M_e^2\right) \quad (11b)$$

where M_e is the external-flow Mach number and r is the wall-temperature recovery factor. Temperature profiles are evaluated using the adiabatic wall law established by Crocco[64,44]:

$$T = T_e\left\{1 + r\frac{\gamma - 1}{2}M_e^2[1 - (u/u_e)^2]\right\} \quad (11c)$$

where T_e is the external-flow static temperature.

For the initialization of k and ε, local turbulence equilibrium was assumed so that[65]

$$k = \left[\frac{\partial u}{\partial y}\right]^2\frac{\ell_m^2}{C_\mu^{1/2}} + k_e\frac{y}{\delta} \quad (12a)$$

$$\varepsilon = C_\mu^{3/4}k^{3/2}/\ell_m + \varepsilon_e\frac{y}{\delta} \quad (12b)$$

where k_e and ε_e are the external-flow values and ℓ_m is the mixing length[64]:

$$\ell_m = \min(0.41y, 0.09\delta) \quad (13)$$

In all of the computations presented in this paper, an external-flow turbulence intensity[44] of 0.1% was used.

Boundary Conditions

The mathematical theory of incompletely parabolic systems of partial differential equations[66,67] indicates criteria concerning the number and type of boundary conditions for the unsteady compressible Navier-Stokes equations. However, usually Euler-type boundary conditions are applied virtually everywhere except at solid boundaries.[68,69] This approach is used in the present study also. Boundary conditions everywhere, except at solid walls, are applied using the compatibility relations method.[61,70] At inflow and outflow boundaries, a one-dimensional nonreflecting boundary condition is applied.[71] On solid walls, the values of both velocity components and of wall temperature or heat flux are imposed. Then the wall pressure is computed using the normal-to-the-wall momentum equation.[72]

The boundary conditions used for the k-ε equations were quite simple. The values of k and ε were imposed at inflows and extrapolated at outflows. Both k and ε were set to zero on solid walls.[12-14,17]

Comparison with Experimental Results

In order to validate the method just presented, comparisons with experimental data from three well-authenticated shock-wave/turbulent-boundary-layer interaction flows[73] (Table 2) were undertaken. Flows I and II (Fig. 2) occur in a symmetric channel on both walls of which interchangeable half-profiles were mounted. Flow III (Fig. 2) is produced in a nonsymmetric channel where a half-profile is mounted on the lower wall of the wind-tunnel test section, the upper wall being straight and slightly convergent streamwise. The trailing-edge details of the three half-profiles (Fig. 2) are significant in that the half-profile is smoothly faired to the wall for flows I and II, but has an abrupt end with a steep descending slope for flow III. This feature of flow III was introduced on purpose[73] in order to induce a large separation.

In internal transonic flows, it is quite possible, contrary to the case of unbounded flows,[36,53] to adjust the back-pressure level so as to fit the computed shock wave at the experimental location. Then, eventual deficiencies of turbulence modeling may be assessed considering the discrepancies between computational and experimental static-to-total pressure ratio. In the present work back-pressure was fixed to get the correct shock-wave position.

Computations of flow I were performed on a 177 × 97 grid, which resolved half of the symmetric channel. The grid was clustered near the wall using geometric-progression spacing, with the first grid point away from the wall being located at $y^+ = 0.2$ at the inflow station. The computed iso-Machs (Fig. 3) clearly indicate the boundary-layer thickening after the interaction with the shock wave, while there is no discernible recirculation region. This feature is in agreement with measurements where it was established that the boundary layer becomes incipiently separated, but remains attached. Comparison of computed and measured mean velocity pro-files (Fig. 3) is satisfactory, although computed profiles downstream of interaction relax somehow slower than the measured ones. The agreement is also quite satisfactory in what concerns the turbulent kinetic energy, although the computed level of turbulent kinetic energy is consistently lower than the measured level downstream of interaction. Globally, flow I is quite accurately predicted.

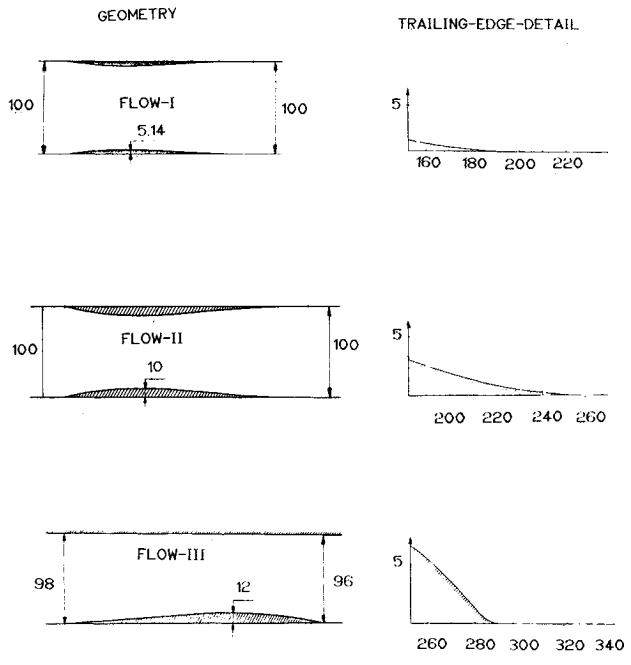

Fig. 2 Geometry of the cases studied and trailing-edge details (all dimensions in millimeters).

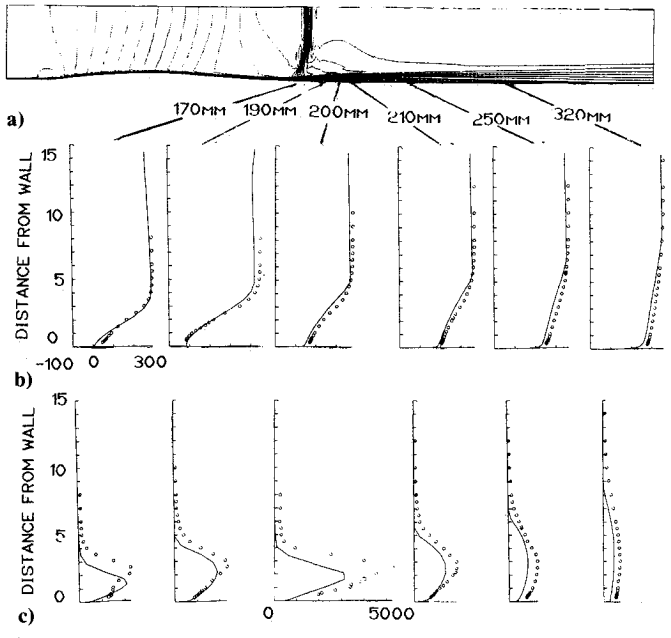

Fig. 3 Flow I comparison between computation and experiment (lengths in millimeters) (● experiment,[73] —— computation): a) iso-Machs; b) mean velocity profiles (m/s); and c) turbulence kinetic-energy profiles (m^2/s^2).

Table 2 Experimental flow description[a]

Flow	M_{sh}	$H_{i_{max}}$	$Re_{\theta_{sh}}$, $\times 10^4$	χ, mm	$p_{t_{inflow}}$, bar	$T_{t_{inflow}}$, K	$\Delta\pi_{S\text{-}T}$, %
I	1.30	~4	0.20	132	0.96	300	<2
II	1.45	~7	0.31	180	0.96	300	<3
III	1.36	~40	0.38	286	0.96	300	<3

[a] M_{sh} = shock Mach number; H_i = maximum incompressible shape factor [Eq. (15)]; Re_θ = Reynolds number at the beginning of the interaction based on boundary-layer momentum thickness; χ = half-profile chord; $p_{t_{inflow}}$ = inflow total pressure; $T_{t_{inflow}}$ = inflow total temperature; and $\Delta\pi_{S\text{-}T}$ = static-to-total channel pressure ratio difference between computation and experiment.

Using a similar approach for flow II, the computed iso-Machs (Fig. 4) indicate a substantial boundary-layer thickening after the interaction with the shock wave. The shock-wave Mach number is 1.45 for flow II, compared with 1.30 for flow I, and this causes the boundary layer to detach after the interaction. The recirculation zone is visible on the iso-Machs plot (Fig. 4). The boundary-layer separation induces a λ shock system (Fig. 4). Comparison of computed and measured mean velocity profiles is again satisfactory. The boundary-layer thickening is correctly predicted for the initial part of the interaction, where the flow is driven by the external-flow pressure gradient. Nevertheless, agreement is poorer in the final part of the interaction, where the boundary layer starts relaxing. Computed profiles far downstream of interaction again relax slower than measured ones. This behavior is easier to understand when considering the turbulent kinetic energy profiles (Fig. 4). There is a consistent underestimation of the turbulence kinetic-energy level in the computations, the model failing to predict adequately the intense turbulence production which takes place during the interaction. This is typical of the k-ε model and has been reported by various researchers.[24,53-55,74]

Computations of flow III were performed on a 193 × 177 grid, which resolved the entire nonsymmetric channel. The grid was geometrically clustered at the vicinity of both walls, the first grid point away from the wall being at $y^+ = 0.2$ at the inflow station. Examination of the computed iso-Machs (Fig. 5) reveals the substantial boundary-layer thickening after the interaction and an important low-momentum region just downstream the trailing edge. Also, the markedly different structure of the shock-wave/turbulent-boundary-layer interaction on the upper wall should be noted. The shock is relatively strong ($M_{sh} = 1.36$) but it does not induce separation on the upper wall, which has zero curvature. On the contrary, the lower-wall curvature is such as to induce separation in a way analogous to backward-facing-step flows.[74-76] Comparison of computed and measured mean velocity profiles (Fig. 5) shows that the experimentally observed extended separation is not satisfactorily predicted. As a consequence, the thickening of the boundary layer downstream of the interaction is seriously underestimated. This is associated with the important underestimation of turbulence kinetic-energy level (Fig. 5).

A more synthetic view of the results is obtained by considering the isentropic wall-Mach-number distribution for the three flows (Fig. 6), given by

$$M_{is} = \left\{ \frac{2}{\gamma - 1} [(p_t/p_{wall})^{(\gamma-1)/\gamma} - 1] \right\}^{1/2} \tag{14}$$

Flow I is accurately predicted with only a slight error in $\pi_{S\text{-}T}$ (<2%). Flow II is also rather well predicted. However, the pressure plateau, typical of the λ shock structure is not sufficiently well resolved by the model. Nevertheless, globally there is good agreement, $\pi_{S\text{-}T}$ being slightly different when compared to the experimental value (<3%). On the contrary, flow III is not well predicted. The large separation, observed experimentally, induces a pronounced pressure plateau, which was not predicted by the model. Nevertheless, the errror in $\pi_{S\text{-}T}$ is not as important (<3%). These conclusions are corroborated by the comparison of computed and measured boundary-layer shape-factor distributions (Fig. 6), this

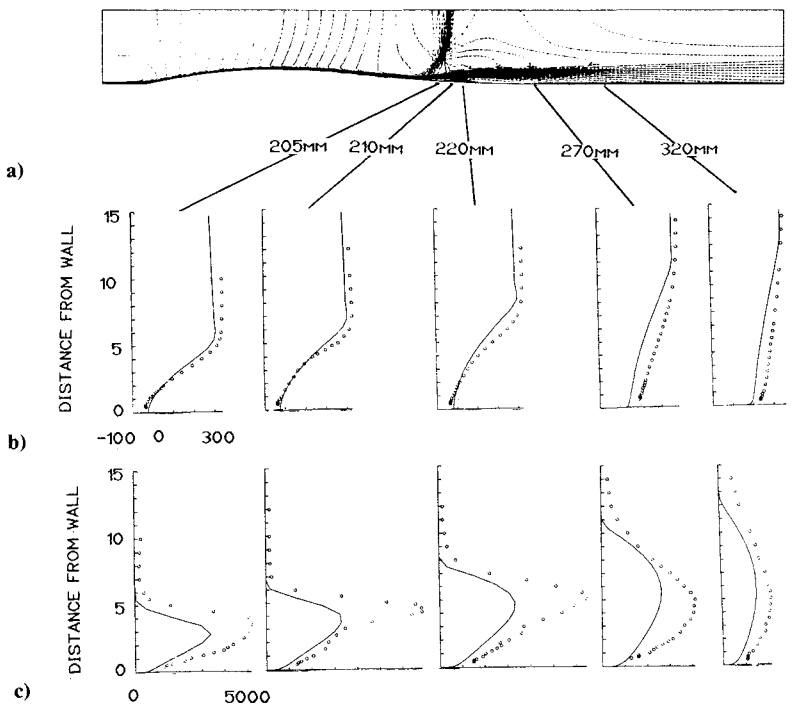

Fig. 4 Flow II comparison between computation and experiment (lengths in millimeters) (• experiment,[73] —— computation): a) iso-Machs; b) mean velocity profiles (m/s); and c) turbulence kinetic-energy profiles (m^2/s^2).

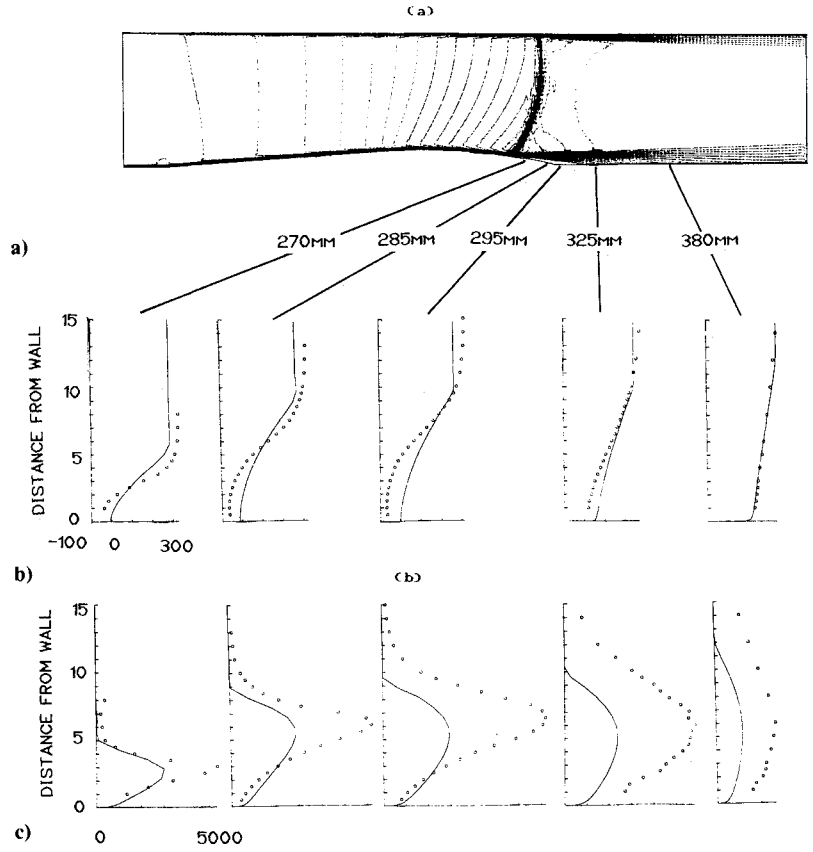

Fig. 5 Flow III comparison between computation and experiment (lengths in millimeters) (• experiment,[73] —— computation): a) iso-Machs; b) mean velocity profiles (m/s); and c) turbulence kinetic-energy profiles (m^2/s^2).

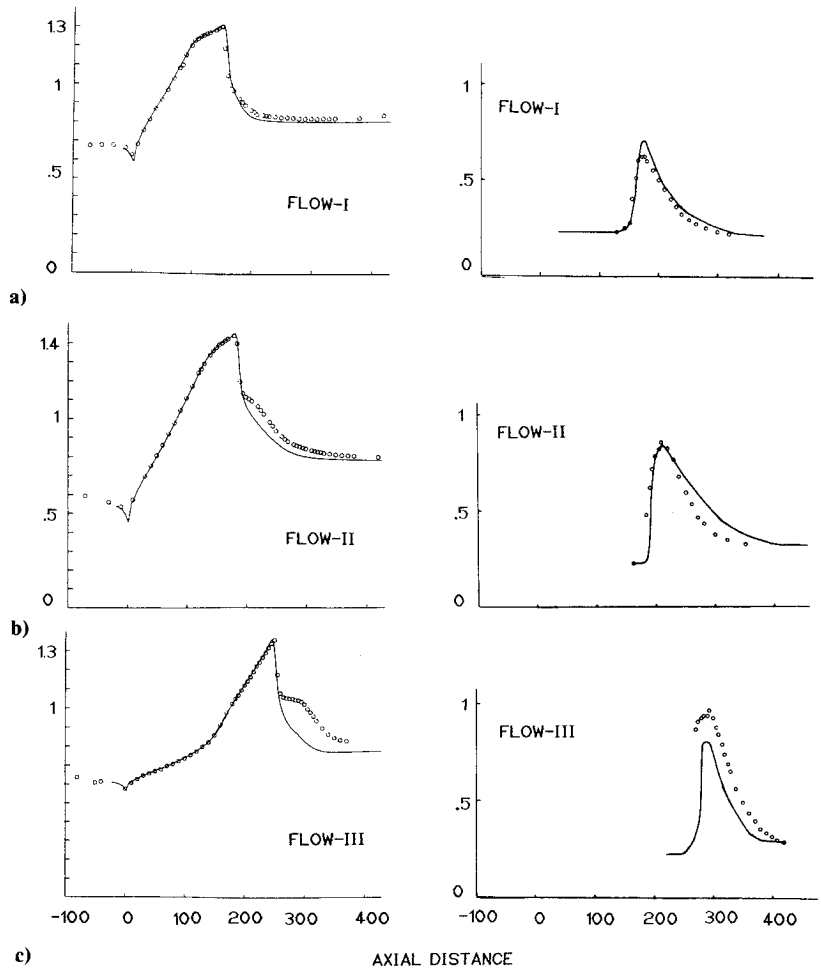

Fig. 6 Comparison of computation with experiment for the three flows (• experiment,[73] —— computation): a) isentropic wall-Mach-number distributions [Eq. (14)] and b) boundary-layer shape-parameter distributions [Eq. (15)].

Table 3 Convergence and computing time requirements

Technique	CPU, min/3000 iterations	CPU, min to convergence
Explicit LTS[a]	217.66	Not reached
Explicit LTS[a] + MLTGRD[b]	262.22	525.32
LTS[a] + MLTGRD[b] + IRS[c]	332.65	332.65

[a]Local time step. [b]Multiple grid. [c] Implicit residual smoothing.

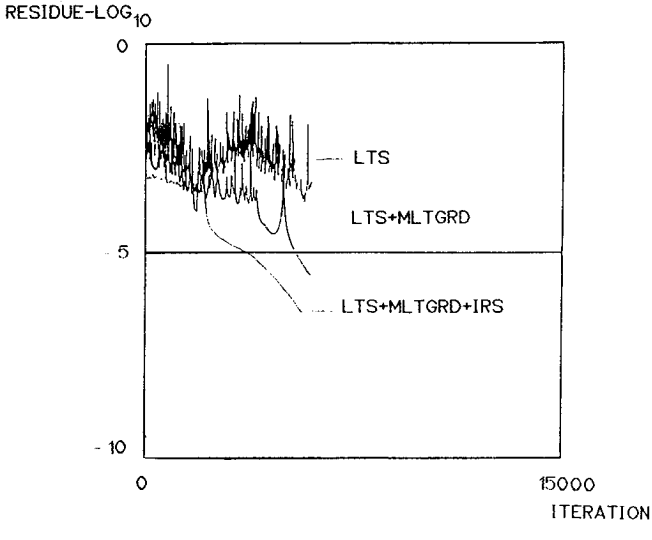

Fig. 7 Comparative convergence history for various combinations of convergence acceleration techniques (see Table 3). LTS = local time step; MLTGRD = multiple grid; and IRS = implicit residual smoothing.

parameter being significant in describing the behavior of the boundary layer[73,77]:

$$J_i = 1 - \frac{1}{H_i} = 1 - \frac{1}{\delta_1^*/\theta_i}$$

$$= 1 - \frac{1}{\left[\int_0^\delta (1 - u/u_e)\,dy\right] \Big/ \left[\int_0^\delta [(1 - u/u_e)u/u_e]\,dy\right]} \quad (15)$$

where H_i is the incompressible shape factor, J_i the incompressible shape parameter, δ_i^* the kinematic displacement thickness, and θ_i the kinematic momentum thickness. Separation usually occurs at $J_i = 0.65 \div 0.75$ or equivalently at $H_i = 3 \div 4$. It is seen that flow I remains attached, and flow II exhibits separation. For both of these flows, agreement between computation and experiment is quite satisfactory. For flow III, the computations predict separated flow but underestimate the extent of the separated region.

It is significant to assess the reasons for the poor success of the k-ε model in predicting flow III, when compared with flow II. The difference is that, for flow II, separation is induced by a rather strong shock wave ($M_{sh} = 1.45$), when for flow III the

shock wave is weaker ($M_{sh} = 1.36$) and separation is primarily induced by the geometry of the trailing edge (Fig. 2). It seems that the influence of streamline curvature[78] is not well modeled. As a general conclusion, the k-ε turbulence model used in the present work does quite well in predicting pressure-driven flows but does less so for relaxing flows.

Convergence and Computing-Time Requirements

In order to depict the advantages from using a complicated multiple-grid scheme with implicit residual smoothing, the convergence for flow I using a 193×177 grid is presented in Fig. 7 for different combinations of schemes. Using only local time steps as convergence acceleration technique results in quite slow convergence rates. There is dramatic convergence acceleration using multiple-grid techniques with very small extra computational effort per iteration (Table 3). The use of implicit residual smoothing enhances convergence (Fig. 7). The multiple-grid technique reaches a 10^{-4} residue in 6000 iterations (Fig. 7). When using implicit residual smoothing on every grid, a 10^{-4} residue is reached in 3000 iterations (Fig. 7), with only 27% more computational effort per iteration (Table 3), so that in terms of convergence computing time the implicit residual-smoothing technique is twice as fast as the explicit one. All of the computations reported in the present work were performed on an AMDAHL-5860 computer.

Conclusions

In the present work, a numerical method is developed for solving the compressible Navier-Stokes equations using k-ε turbulence closure with low Reynolds number and near-wall effects. It uses an explicit, implicitly smoothed, multiple-grid algorithm. The implementation of the k-ε model was successful in not altering the time steps used for the integration of the Navier-Stokes equations, when compared with algebraic turbulence closures. The use of implicit residual smoothing on every grid significantly improves the convergence rate.

In order to substantiate the validity of the method, comparisons with experimental data from three shock-wave/turbulent-boundary-layer interaction flows were undertaken. Notwithstanding the fact that the classical drawbacks of the k-ε model, namely in predicting relaxing flows or flows with important streamline curvature, introduced discrepancies, the comparison was globally satisfactory.

One important conclusion that is drawn from the present work is that it is quite possible to use k-ε closure in efficient time-marching computational algorithms, without degrading neither stability nor convergence-rate characteristics, contrary to the generally accepted opinion.

It is believed that algorithm convergence rate and computing-time requirements may still be enhanced by using implicit residual smoothing and multigrid techniques, more elaborated than the ones used in the present study. Also, the use of implicit boundary conditions would probably be beneficial. Improvements in turbulence closure are necessary in order to predict accurately flows with large separation and important streamline curvature.

Acknowledgments

This work was conducted at the Combustion Department of SNECMA and is published with the permission of the direction of SNECMA. Cambier of ONERA-Châtillon provided a constant enthalpy mixing-length explicit multiple-grid Navier-Stokes code[50] from which the present code evolved. Délery of ONERA-Meudon provided enlightening comments on the experimental data used to validate the method.

References

[1]Kutler, P., Steger, J. L., and Bailey, F. R., "Status of Computational Fluid Dynamics in the United States," AIAA Paper 87-1135, 1987.

[2]Henningson, D., Spalart, P., and Kim, J., "Numerical Simulation of Turbulent Spots in Plane Poiseuille and Boundary-Layer Flow," *Physics of Fluids*, (to appear).

[3]Moin, P., and Kim, S., "The Structure of the Vorticity Field in Turbulent Channel Flows. Pt. 1. Analysis of Instantaneous Fields Statistical Correlations," *Journal of Fluid Mechanics*, Vol. 155, 1985, pp. 441–464.

[4]Kim, J., and Moin, P., "The Structure of the Vorticity Field in Turbulent Channel Flows. Pt. 2. Study of Ensemble-Averaged Fields," *Journal of Fluid Mechanics*, Vol. 162, 1986, pp. 339–363.

[5]Shang, J. S., "An Assessment of Numerical Solutions of the Complete Navier-Stokes Equations," *Journal of Aircraft*, Vol. 22, May 1985, pp. 353–370.

[6]Chapman, D. R., "Computational Aerodynamics Development and Outlook," *AIAA Journal*, Vol. 17, Dec. 1979, pp. 1293–1315.

[7]Kutler, P., "A Perspective of Theoretical and Applied Computational Fluid Dynamics," *AIAA Journal*, Vol. 23, March 1985, pp. 328–341.

[8]Johnson, D. A., and King, L. S., "A Mathematically Simple Turbulence Closure Model for Attached and Separated Turbulent Boundary-Layers," *AIAA Journal*, Vol. 23, Nov. 1985, pp. 1685, pp. 1685–1692.

[9]Reynolds, W. C., "Computation of Turbulent Flows," *Annual Review of Fluid Mechanics*, Vol. 8, 1976, pp. 183–208.

[10]Launder, B. E., "Computational Modeling of Turbulent Flows," *Advances in Applied Mechanics*, Vol. 18, 1978, pp. 123–176.

[11]Launder, B. E., "Numerical Computation of Convective Heat Transfer in Complex Turbulent Flows: Time to Abandon Wall Functions?," *International Journal of Heat and Mass Transfer*, Vol. 27, 1984, pp. 1485–1491.

[12]Jones, W. P., and Launder, B. E., "The Prediction of Laminarization with a Two-Equation Model of Turbulence," *International Journal of Heat and Mass Transfer*, Vol. 15, 1972, pp. 301–314.

[13]Jones, W. P., and Launder, B. E., "The Prediction of Low-Reynolds-Number Phenomena with a Two-Equation Model of Turbulence," *International Journal of Heat and Mass Transfer*, Vol. 16, 1973, pp. 1119–1130.

[14]Launder, B. E., and Sharma, B. I., "Application of the Energy Disipation Model of Turbulence to the Calculation of Flows near a Spinning Disk," *Letters in Heat and Mass Transfer*, Vol. 1, 1974, pp. 131–138.

[15]Hinze, O., *Turbulence*, McGraw-Hill, New York, 1979, pp. 15–29.

[16]Speziale, C. G., "On Nonlinear k-ℓ and k-ε Models of Turbulence," *Journal of Fluid Mechanics*, Vol. 178, 1987, pp. 459–475.

[17]Patel, V. C., Rodi, W., and Scheuere, G., "Turbulence Models for Near-Wall and Low-Reynolds-Number Flows: A Review," *AIAA Journal*, Vol. 23, Sept. 1985, pp. 1308–1319.

[18]Chien, K. Y., "Prediction of Channel and Boundary-Layer Flows with a Low-Reynolds-Number Turbulence Model," *AIAA Journal*, Vol. 20, Jan. 1982, pp. 33–38.

[19]Lam, C. K. G., and Bremhorst, K., "A Modified Form of the k-ε Model for Predicting Wall Turbulence," *ASME Journal of Fluids Engineering*, Vol. 103, Sept. 1981, pp. 456– .

[20]Wilcox, D. C., and Rubesin, M. W., "Progress in Turbulence Modeling for Complex Flowfields Including the Effects of Compressibility," NASA TP 1517, 1980.

[21]Bernard, P. S., "Limitations of the Near-Wall k-ε Turbulence Model," *AIAA Journal*, Vol. 24, April, 1986, pp. 619–622.

[22]Rotta, J. "Statistische Theorie nichthomogener Turbulenz. 1. Mitteilung," *Zeitschrift fuer Physik*, Vol. 129, 1951, pp. 547–572.

[23]Lakshminarayana, B., "Turbulence Modeling for Complex Shear Flows," *AIAA Journal*, Vol. 24, Dec. 1986, pp. 1900–1917.

[24]Nallasamy, M., "A Critical Evaluation at Various Turbulence Models as Applied to Internal Fluid Flows," NASA TP 2474, 1985.

[25]Beam, R. M., and Warming, R. F., "An Implicit Factored Scheme for the Compressible Navier-Stokes Equations," *AIAA Journal*, Vol. 16, April 1978, pp. 393–402.

[26]Greenberg, J. B., "Semi-implicit Hopscotch-Type Methods for the Time-Dependent Navier-Stokes Equations," *AIAA Journal*, Vol. 20, Aug. 1982, pp. 1064–1070.

[27]Reklis, R. P., and Thomas, P. D., "Shock-Capturing Algorithm for the Navier-Stokes Equations," *AIAA Journal*, Vol. 20, Sept. 1982, pp. 1212–1218.

[28]Knight, D. D., "A Hybrid Explicit-Implicit Numerical Algorithm for the 3-D Compressible Navier-Stokes Equations," *AIAA Journal*, Vol. 22, Aug. 1984, pp. 1056–1063.

[29]Wornom, S. F., and Hafez, M. M., "Implicit Conservative Schemes for the Euler Equations," *AIAA Journal*, Vol. 24, Feb. 1986, pp. 215–223.

[30]Walters, R. W., Dwoyer, D. L., and Hassan, H. A., "A Strongly Implicit Procedure for the Compressible Navier-Stokes Equations," *AIAA Journal*, Vol. 24, Jan. 1986, pp. 6–12.

[31]Crocco., L., "A Suggestion for the Numerical Solution of the Steady Navier-Stokes Equations," *AIAA Journal*, Vol. 3, Oct. 1965, pp. 1824–1832.

[32]Lomax, H., "Some Prospects for the Future of Computational Fluid Dynamics," *AIAA Journal*, Vol. 20, Aug. 1982, pp. 1033–1043.

[33]Jameson, A., and Yoon, S., "Multigrid Solution of the Euler Equations Using Implicit Schemes," *AIAA Journal*, Vol. 24, Nov. 1986, pp. 1737–1743.

[34]Jameson, A., and Yoon, S., "Lower-Upper Implicit Schemes with Multiple-Grids for the Euler Equations," *AIAA Journal*, Vol. 25, July 1987, pp. 929–935.

[35]Coackley, T. J., "Turbulence Modeling Methods for the Compressible Navier-Stokes Equations," AIAA Paper 83-1693, 1983.

[36]Johnson, D. A., "Transonic Separated Flow Predictions with an Eddy-Viscosity/Reynolds-Stress Closure Model," *AIAA Journal*, Vol. 25, Feb. 1987, pp. 252–259.

[37]Ni, R. H., "A Multiple-Grid Scheme for Solving the Euler Equations," *AIAA Journal*, Vol. 20, Nov. 1982, pp. 1565–1571.

[38]Davis, R. L., Ni, R. H., and Bowley, W. W., "Prediction of Compressible Laminar Viscous Flows Using a Time-Marching Control-Volume and Multiple-Grid Technique," *AIAA Journal*, Vol. 22, Nov. 1984, pp. 1573–1581.

[39]Lerat, A., "Implicit Methods of Second-order Accuracy for the Euler Equations," *AIAA Journal*, Vol. 23, Jan. 1985, pp. 33–40.

[40]Sides, J., "Calcul d'Ecoulements Transsoniques Instationnaires à l'Aide d'une Méthode Numérique Implicite de Résolution des Equations d'Euler," *Recherche Aérospatiale*, Feb. 1985, pp. 89–111.

[41]Favre, A., "Equations des Gaz Turbulents Compressibles. I. Formes Générales," *Journal de Mécanique*, Vol. 4, Sept. 1965, pp. 361–390.

[42]Favre, A., "Equations des Gaz Turbulents Compressibles. II. Méthode des Vitesses Moyennes; Méthode des Vitesses Moyennes Pondérées par la Masse Volumique," *Journal de Mécanique*, Vol. 4, Dec. 1965, pp. 391–421.

[43]Liepmann, H., and Roshko, A., *Elements of Gasdynamics*, John Wiley and Sons, New York, 1957, pp. 7–10 and pp. 378–380.

[44]Schlichting, H., *Boundary-Layer Theory*, McGraw-Hill, New York, 1979, pp. 327–330, pp. 60–63, pp. 330–339, and pp. 572–574.

[45]Eckert, E. R. G., and Drake, R. M., *Analysis of Heat and Mass Transfer*, McGraw-Hill, New York, 1972, pp. 64–66 and p. 780.

[46]Morkovin, M. V., "Effects of Compressibility on Turbulent Flows," The Colloquium on the Mechanics of Turbulence, Marseille, France, 1964.

[47]Laufer, J., "Thoughts on Compressible Turbulent Boundary Layers," NASA SP 216, 1969, pp. 1–13.

[48]Vandromme, V., and Haminh, H., "Turbulence Modeling for Compressible Flows," von Kármán Institute, LS 1987-06, 1987.

[49]Sahu, J., and Danberg, J. E., "Navier-Stokes Computations of Transonic Flows with a Two-Equation Turbulence Model," *AIAA Journal*, Vol. 24, Nov. 1986, pp. 1744–1751.

[50]Cambier, L., Couailler, V., and Veuillot, J. P., "Numerical Solution of the Navier-Stokes Equations by a Multigrid Method," *Recherche Aérospatiale*, Vol. 1988, March 1988, pp. 23–42.

[51]Pulliam, T. H., "Artificial Dissipation Models for the Euler Equations," *AIAA Journal*, Vol. 24, Dec. 1986, pp. 1931–1940.

[52]Johnson, G. M., "Multiple-Grid Convergence Acceleration of Viscous and Inviscid Flow Computations," *Applied Mathematics and Computation*, Vol. 13, 1983, pp. 375–398.

[53]Viegas, J. R., and Horstmann, C. C., "Comparison of Multiequation Turbulence Models for Several Shock/Boundary-Layer Interaction Flows," *AIAA Journal*, Vol. 17, Aug. 1979, pp. 811–820.

[54]Escande, B., and Cambier, L., "Turbulence Modeling in Transonic Interaction," presented at the Turbulent Shear-Layer/Shock-Wabe Interactions IUTAM Symposium, Palaiseau, France, 1985.

[55]Degrez, G., and Vandromme, D., "Implicit Navier-Stokes Calculations of Transonic Shock/Turbulent Boundary-Layer Interactions," presented at the Turbulent Shear-Layer/Shock-Wave Interactions IUTAM Symposium, Palaiseau, France, 1985.

[56]Jameson, A., and Mavriplis, D., "Finite-Volume Solution of the Two-Dimensional Euler Equations on a Rectangular Triangular Mesh," *AIAA Journal*, Vol. 24, April 1986, pp. 611–618.

[57]Thompson, J. F., Thames, F. C., and Mastin, W., "Automatic Numerical Generation of Boddy-Fitted Curvilinear Coordinate System for the Field Containing any Number of Arbitrary Two-Dimensional Bodies," *Journal of Computational Physics*, Vol. 15, 1974, pp. 299–319.

[58]Warzi, Z. U. A., "Generation of Three-Dimensional Grids Through Elliptic Differential Equations," von Kármán Institute, LS 1984-04, 1984.

[59]Roache, P. J., *Computational Fluid Dynamics*, Hermosa, Albuquerque, New Mexico, 1976, pp. 106–109.

[60]Rhie, C. M., and Chow, W. L., "Numerical Study of the Turbulent Flow Past an Airfoil with Trailing-Edge Separation," *AIAA Journal*, Vol. 21, Nov. 1983, pp. 1525, 1532.

[61]Veuillot, J. P., and Cambier, L., "A Subdomain Approach for the Computation of Compressible Inviscid Flows," ONERA TP 1984-61, 1984.

[62]Kuhn, G. D., and Nielsen, J. N., "An Analytical Method for Calculating Turbulent Separated Flows Due to Adverse Pressure Gradients," Project SQUID TR NEAR-1-PU, 1971.

[63]Maise, G., and McDonald, H., "Mixing Length and Kinematic Eddy Viscosity in Compressible Boundary Layers," *AIAA Journal*, Vol. 6, Jan. 1968, pp. 73–80.

[64]Van Driest, E. R., "Turbulent Boundary Layers in Compressible Fluids," *Journal of the Aeronautical Sciences*, Vol. 18, March 1951, pp. 145–160.

[65]Wang, J. H., Jen, H. F., and Hartel, E. O., "Airfoil Heat-Transfer Calculation Using a Low-Reynolds-Number Version of a Two-Equation Turbulene Model," *ASME Journal of Engineering for Gas Turbines and Power*, Vol. 107, Jan. 1985, pp. 60–67.

[66]Strikwerda, J. C., "Initial-Boundary-Value Problems for Incompletely Parabolic System," *Communications on Pure and Applied Mathematics*, Vol. 30, 1977, pp. 797–822.

[67]Gustatson, B., and Sundström, A., "Incompletely Parabolic Problems in Fluid Dynamics," *SIAM Journal of Applied Mathematics*, Vol. 35, Sept. 1976, pp 343–357.

[68]Rudy, D. H., and Strikwerda, J. C., "A Nonreflecting Outflow Boundary Condition for Subsonic Navier-Stokes Calculations," *Journal of Computational Physics*, Vol. 36, 1980, pp. 55–70.

[69]Rudy, D. H., and Strikwerda, J. L., "Boundary Conditions for Subsonic Compressible Navier-Stokes Calculations," *Computers and Fluids*, Vol. 9, 1981, pp. 327–338.

[70]Veuillot, J. P., and Meauzé, G., "A 3-D Euler Method for Internal Transonic Flows Computation with a Multidomain Approach," AGARD LS 140, 1985, 5.1–5.21.

[71]Hedström, G. W., "Nonreflecting Boundary Conditions for Linear Hyperbolic Systems," *Journal of Computational Physics*, Vol. 30, 1979, pp. 222–237.

[72]Benocci, C., and Michelassi, V., "The Influence of the Wall Boundary Conditions on a Solution of the Incompressible Navier-Stokes Equations," von Kármán Institute, TM 42, 1986.

[73]Délery, J. M., "Experimental Investigation of Turbulence Properties in Transonic Shock/Boundary-Layer Interactions," *AIAA Journal*, Vol. 21, Feb. 1983, pp. 180–185.

[74]Benay, R., Coet, M. C., and Délery, J., "Turbulence Model Validation Applied to Transonic Shock-Wave/Boundary-Layer Interaction," *Recherche Aérospatiale*, Vol. 1987, May 1987, pp. 1–16.

[75]Kim, J., Kline, S. J., and Johnston, J. P., "Investigation of a Reattaching Turbulent Shear Layer: Flow over a Backward-Facing Step," *ASME Journal of Fluids Engineering*, Vol. 102, Sept. 1980, pp. 302–308.

[76]Driver, D. M., and Seegmiller, H. L., "Features of a Reattaching Turbulent Shear Layer in Divergent Channel Flow," *AIAA Journal*, Vol. 23, Feb. 1985, pp. 163–174.

[77]Gerolymos, G. A., Kallas, Y. N., and Papailiou, K. D., "The Behavior of the Normal Fluctuation Terms in the Case of Attached and Detached Turbulent Boundary Layers," *Revue de Physique Appliquée*, Vol. 24, March 1989, pp. 375–387.

[78]Bradshaw, P., "The Analogy between Streamline Curvature and Buoyancy in Turbulent Shear Flow," *Journal of Fluid Mechanics*, Vol. 36, 1969, pp. 177–191.